Cytometry
PART A
Journal of the International Society for Advancement of Cytometry

MIFlowCyt

Cluster Cytometry for High-Capacity Bioanalysis

Bruce S. Edwards,[1,2]* Jingshu Zhu,[3] Jun Chen,[2] Mark B. Carter,[2] David M. Thal,[4] John J.G. Tesmer,[4] Steven W. Graves,[3] Larry A. Sklar[1,2]

[1]Department of Pathology, University of New Mexico, Albuquerque, New Mexico

[2]Center for Molecular Discovery, University of New Mexico, Albuquerque, New Mexico

[3]Center for Biomedical Engineering, University of New Mexico, Albuquerque, New Mexico

[4]Life Sciences Institute, University of Michigan, Ann Arbor, Michigan

Received 11 November 2011; Revision Received 7 February 2012; Accepted 19 February 2012

Additional Supporting Information may be found in the online version of this article.

Presented in part at the ISAC CYTO10 Congress, Seattle, WA, May, 2010 and the Biopharmaceutical Flow Cytometry and Imaging Conference, GlaxoSmithKline, Ware, UK, October, 2010.

Conflict of interest: B.S.E. and L.A.S. are coinventors of the HyperCyt high-throughput flow cytometry platform and cofounders of IntelliCyt Corporation, Albuquerque, NM, the commercial manufacturer and distributor of the HyperCyt platform.

Grant sponsor: NIH; Grant numbers: R01HG005066, U54MH084690, R03MH093184-01A1, R03 DA030557-01A1, R01 HL071818; Grant sponsors: The University of New Mexico Center for Molecular Discovery and University of New Mexico Cancer Center Shared Flow Cytometry and High Throughput Screening Resource;

ISAC
International Society for Advancement of Cytometry

Abstract

Flow cytometry specializes in high-content measurements of cells and particles in suspension. Having long excelled in analytical throughput of single cells and particles, only recently with the advent of HyperCyt sampling technology, flow cytometry's multiexperiment throughput has begun to approach the point of practicality for efficiently analyzing hundreds-of-thousands of samples, the realm of high-throughput screening (HTS). To extend performance and automation compatibility, we built a HyperCyt-linked Cluster Cytometer platform, a network of flow cytometers for analyzing samples displayed in high-density, 1,536-well plate format. To assess the performance, we used cell- and microsphere-based HTS assays that had been well characterized in the previous studies. Experiments addressed important technical issues: challenges of small wells (assay volumes 10 μL or less, reagent mixing, cell and particle suspension), detecting and correcting for differences in performance of individual flow cytometers, and the ability to reanalyze a plate in the event of problems encountered during the primary analysis. Boosting sample throughput an additional fourfold, this platform is uniquely positioned to synergize with expanding suspension array and cell barcoding technologies in which as many as 100 experiments are performed in a single well or sample. As high-performance flow cytometers shrink in cost and size, cluster cytometry promises to become a practical, productive approach for HTS, and other large-scale investigations of biological complexity.

Key terms

flow cytometry; suspension array; high-content analysis; high-throughput screening

Introduction

Microscope imaging-based high-content screening (HCS) platforms revolutionized the drug discovery enterprise when introduced in the late 1990s, bridging the gap between throughput and information richness of experiments performed with adherent cells (1). Imaging-based HCS technology has improved and expanded over subsequent years to become considered a mainstream screening technology in the pharmaceutical industry (2). Flow cytometry is a complementary technology that specializes in high-content measurements of suspension cells such as leukocytes and hematopoetic stem cells. It measures multiple optical signals associated with cells or particles as they pass through a laser-based detection system, one at a time. Flow cytometry has long excelled in throughput and information density for the analysis of individual cells, now routinely capable of quantifying 16 or more features per cell at tens-of-thousands of cells per second. However, only recently with the introduction of HyperCyt sampling technology it has begun to achieve levels of multiexperiment throughput compatible with its application in a high-throughput screening (HTS) environment (3–5).

HyperCyt uses a peristaltic pump in combination with an autosampler to boost throughput of experimental samples 10- to 20-fold (3). The autosampler moves a sample uptake probe from well to well of a multiwell microplate, whereas the continuously running pump causes uptake of a 1–2 μL sample from each well and an air

*Correspondence to: Bruce S. Edwards, Center for Molecular Discovery, University of New Mexico Health Sciences Center, CRF217, MSC11-6020, Albuquerque, NM 87131, USA

Email: bedwards@salud.unm.edu

Published online 21 March 2012 in Wiley Online Library (wileyonlinelibrary.com)

DOI: 10.1002/cyto.a.22039

bubble to separate each sample from the other. Samples from all wells of a microplate are delivered to the flow cytometer in a single round of analysis and stored in a single data file. Specialized software distinguishes and extracts data for individual samples by virtue of temporal gaps in the flow of cells, resulting from passage of the sample-separating air bubbles through the laser beam.

The platform has been extensively validated for producing high content, quantitative measurements while processing 384-well plates in 11 min or less (6–20). It has been successfully used in small-molecule screening assays to produce more than 10 million experimental measurements of small molecule interactions with biological targets, all published on the publically accessible PubChem website (www.ncbi.nlm.nih.gov/pcassay). The conventional HyperCyt platform, of which there are currently more than 100 in laboratories worldwide, is linked to a single flow cytometer and typically processes ~ 15,000 wells/day. To achieve throughput compatible with screening of libraries containing several hundred thousand compounds or more, it has been necessary to use up to four separate platforms running in parallel. This is an expensive and labor-intensive approach that requires significant institutional space and complex logistics of operation that are not readily amenable to full automation. To improve performance efficiency and automation compatibility, we built and tested a Cluster Cytometer HyperCyt platform that is capable of analyzing samples displayed in high-density, 1,536-well plate format.

Materials and Methods

Cells and Reagents

Myeloid U937 cells transfected with the human formyl-peptide receptor (FPR) were cultured in RPMI-1640 medium (Mediatech, Manassas, VA; 15-041-CV) supplemented with 10% heat-inactivated fetal bovine serum (GIBCO, Grand Island, NY; 14160), 2 mM L-glutamine-10 U/mL penicillin-10 μg/mL streptomycin (Omega Scientific, Tarzana, CA; PG-30), 10 mM HEPES (Sigma, St. Louis, MO; H-0887), and 4 μg/mL Ciproflaxin (Mediatech MT61-277-RF). Cultures were grown at 37°C in a 5% CO_2 atmosphere, and passaged every 3 days. U937 cells were used that expressed a mutant FPR with glycine and alanine substituted for serine and threonine residues in the C-terminal tail (DeltaST) to prevent receptor internalization (21). Peptide dilution buffer (PDB) consisted of 110 mM NaCl (Sigma S-9625), 30 mM HEPES, 10 mM KCl (Sigma P-3911), 1 mM $MgCl_2$ (Sigma M-8266), 10 mM glucose (Sigma G-8270), and 0.1% bovine serum albumin (Sigma B-2518). Protease buffer consisted of 50 mM HEPES, 100 mM NaCl, 1 mg/mL bovine serum albumin, 0.025% Tween-20 (Sigma P-7949), pH 7.4. *N*-formyl-methionine-leucine-phenylalanine-phenylalanine peptide (fMLFF) was obtained from Sigma (F-3506). Fluorescein-labeled tryptophan–lysine–tyrosine–methionine–valine–D-methionine (WPEP–FITC) was obtained from New England Peptide (Gardner, PA; custom synthesis) and was previously characterized (22). Multiplexed sets of streptavidin-coated microspheres were obtained from Spherotech (Lake Forest, IN; Blue array particle kit, 5.1 μm, SVPAK500-5067-X-4). Quantum FITC molecules of equivalent soluble fluorescein (MESF) low-level and high-level fluorescein calibration standard microspheres were obtained from Bangs Laboratories (Fishers, IN; 824B and 825B, respectively). Recombinant *Bacillus anthracis* lethal factor (LF) and *Clostridium botulinum* neurotoxin light chain A (BoNTALC) were obtained from List Laboratories (Campbell, CA; 169A and 610A, respectively). All test compounds were stored in 100% DMSO (Fisher Scientific, Fair Lawn, NJ; D136-1) and diluted 1:100 in each assay so that wells containing test compounds also contain 1% DMSO. Control wells are added with 1% DMSO (vehicle control) to control for potential extraneous effects of DMSO on the assay. A key aspect of assay development is demonstration that the assay output is unaffected by DMSO in amounts expected to be present in test compound containing wells.

Hardware and Software

Accuri C6 flow cytometers equipped with CFlow Plus and CFlow Plus Automation software were obtained from BDAccuri (Ann Arbor, MI). All had the standard configuration of detectors common to most if not all other C6s. Photomultiplier tubes and other detectors were operated at fixed, manufacturer-specified voltages and gains that were not subjected to user modification. The GX274 autosampler and 4-channel peristaltic pump were obtained from Gilson Instruments (Middleton, WI). HyperCyt Autosampler control software (version 2.0, IntelliCyt, Albuquerque, NM) was modified to control the GX274 autosampler and Accuri C6 flow cytometers via RS232 serial port and Ethernet TCP/IP network communication, respectively. HyperView software (version 2.5.1, IntelliCyt) was modified to enable linked analysis of the four FCS data files generated by processing of each 1,536-well plate and automated standardization of fluorescence data from curves generated with fluorescein calibration standard microspheres. A Biomek FX robot (Beckman Coulter, Indianapolis, IN) equipped with a 1,536 pintool set containing 100 nL pins (V&P Scientific, San Diego, CA; VP 550A) was used to transfer small molecule test compounds to 1,536-well bioassay plates. A MicroFlo Select dispenser equipped with a 1-μL dispense cassette (BioTek Instruments, Winooski, VT) was

used to dispense cells, microspheres, and reagents into wells. Assays were performed in 1,536-well, HiBase polystyrene plates (MPG-782101; Greiner Bio-One, Monroe, NC).

FPR Ligand-Binding Inhibition Assay

As described previously (23,24), the FPR assay measures the ability of test compounds to compete with a high-affinity fluorescent ligand, WPEP–FITC, for binding to cell membrane FPR. The assay response was quantified on the basis of median green fluorescence intensity (MFI) determinations of cell-bound WPEP–FITC made for individual wells. The assay response range was defined by replicate control wells containing unlabeled fMLFF blocking peptide in PDB (positive controls, with minimum MFI expected from complete inhibition of WPEP–FITC binding) or PDB with 1% DMSO alone (negative controls, with maximum MFI expected from no inhibition of WPEP–FITC binding). For assay performance, additions to wells were in sequence as follows: (1) 375 nM fMLFF or PDB alone (4 μL/well); (2) cells (10^7/mL, 3 μL/well); (3) (after 30 min, 4°C incubation) 17 nM WPEP–FITC (3 μL/well). After an additional 45 min, 4°C incubation, plates were immediately analyzed by flow cytometry with the HyperCyt® platform. All incubations were performed with plates rotating continuously from inverted to upright position to maintain cells in suspension. Test compound inhibition of WPEP–FITC binding to FPR was calculated as $100 \times (MFI_{MAX} - MFI_{TEST})/(MFI_{MAX} - MFI_{MIN})$, in which MFI_{MAX} and MFI_{MIN} represent the averages for MFI determinations in negative and positive control wells, respectively, and MFI_{TEST} represents the MFI measured in wells containing test compounds and WPEP–FITC in combination. Details of gating strategy and an assay schematic are shown in Supporting Information Fig. 3.

Protease Inhibition Assay

Protease inhibition assays were performed as described previously (25), but with modifications. Biotinylated green fluorescent protein (GFP) protease substrates for LF, BoNTALC, and a protease-resistant substrate (pinpointGFP) were prepared and loaded on streptavidin microspheres as described previously (14,25,26). Additions to wells were in sequence as follows: (1) 4 μL protease buffer; (2) 2 μL of a mixture of 1.5 μM LF and 5 nM BoNTALC in protease buffer; (3), 100 nL of test compounds (1 mM in DMSO); and (4) 4 μL containing 2×10^5/mL of each set of substrate-bearing microspheres. Plates were sealed and incubated at 24°C overnight (16–18 h), rotating continuously from inverted to upright position until analyzed in the HyperCyt platform the following day. The assay response was quantified on the basis of MFI determinations of microsphere-bound protease substrate-GFP made for individual wells. The assay response range was defined by replicate control wells containing no proteases (positive controls, with maximum MFI reflecting the expected response from complete protease inhibition) or the protease mixture alone (negative controls, with minimum MFI reflecting complete absence of protease inhibition). Test compound inhibition of substrate cleavage by protease resulted in an increase in MFI relative to negative controls and was calculated as $100 \times (MFI_{TEST} - MFI_{MIN})/(MFI_{MAX} - MFI_{MIN})$, in which MFI_{MIN} and MFI_{MAX} represent the averages for MFI determinations in negative and positive control wells, respectively, and MFI_{TEST} represents the MFI measured in wells containing test compounds and protease mixtures in combination. Details of gating strategy and an assay schematic are shown in Supporting Information Fig. 4.

G Protein-Coupled Receptor Kinase 2 Assay

The G protein-coupled receptor kinase 2 (GRK2) assay measures the ability of test compounds to displace a fluorescently labeled RNA aptamer that binds with nanomolar affinity to the GRK2 protein. GRK2 protein was biotinylated using biotin *N*-hydroxysuccinimide ester (Sigma) and conjugated to streptavidin-coated beads (Spherotech) at 4°C overnight in GRK2 assay buffer (20 mM HEPES, pH 7.0, 10 mM NaCl, 5 mM $MgCl_2$, 0.1% Lubrol, 2 mM DTT, 1 mM CHAPS). The RNA aptamer was fluorescently labeled at a single site on the 3′ end with 6-carboxyfluorescein to produce aptamer-3′-FAM (1 FAM group per RNA aptamer, synthesized, and labeled by IDT (www.IDTDNA.com)), which was diluted to 6.6 nM in GRK2 assay buffer. A total volume of 10 μL was added to wells in the following sequence: (1), 4 μL GRK2 assay buffer; (2), 100 nL of 1 mM test compounds; (3), 3 μL GRK2-conjugated beads, incubated at room temperature for 15 min; and (4), 3 μL 6.6 nM aptamer-3′-FAM. Plates were incubated at room temperature for 1 h, rotating continuously from inverted to upright position. Plates were then analyzed by flow cytometry with the HyperCyt platform. The assay response was quantified on the basis of aptamer-3′-FAM MFI determinations made for individual wells. The assay response range was defined by replicate control wells containing 1% DMSO vehicle control (negative controls, with maximum MFI expected from no inhibition of aptamer-3′-FAM binding) or 50× unlabeled RNA aptamer in assay buffer (positive controls, with minimum MFI expected from complete inhibition of aptamer-3′-FAM binding). Test compound inhibition of aptamer-3′-FAM binding to GRK2 was calculated as $100 \times (MFI_{MAX} - MFI_{TEST})/(MFI_{MAX} - MFI_{MIN})$ in which MFI_{MAX} and MFI_{MIN} represent the averages for MFI determinations in negative and positive control wells, respectively, and MFI_{TEST} represents the MFI measured in wells containing test compounds and aptamer-3′-FAM in combination.

Assay Quality Assessment

In all assays, the mean and standard deviation (SD) of MFI measurements from replicate control wells were used to calculate the Z' score, a dimensionless measure of screening assay quality that reflects both assay signal dynamic range and data variation associated with the signal measurements (27). As illustrated in assay descriptions above, some assays were designed to detect test compound effects that cause an increase in MFI, whereas others were designed to detect MFI

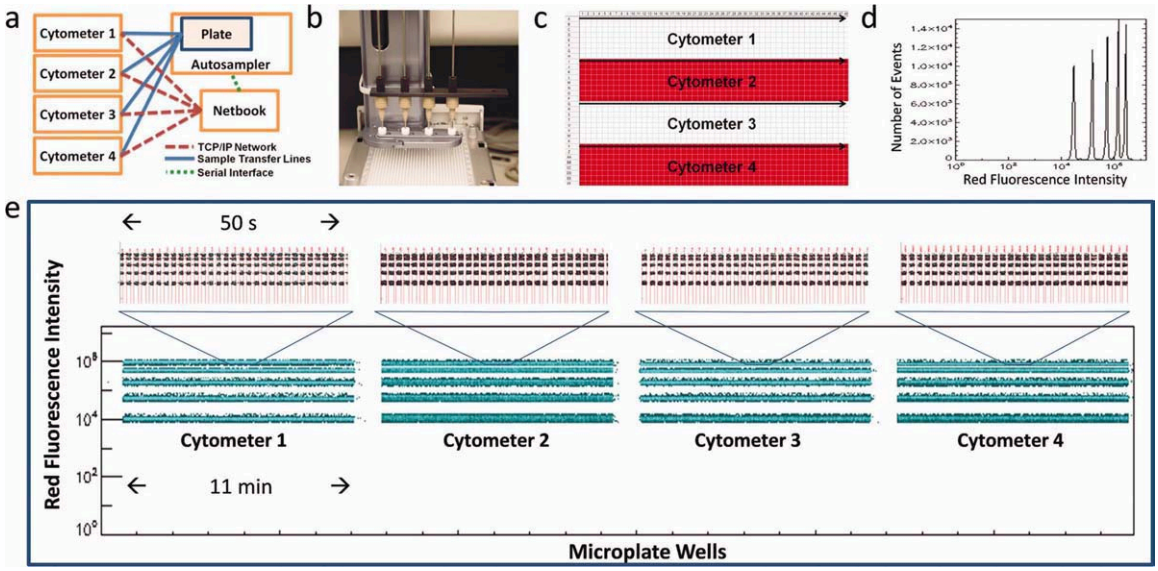

Figure 1. Cluster Cytometer HyperCyt Platform. (**a**) Schematic of the Cluster Cytometer HyperCyt platform illustrating sample transfer lines linking sample uptake ports from each of four flow cytometers to sampling probes positioned above the 1,536-well plate (solid lines), and serial (small dashed lines) and Ethernet network (large dashed lines) connections by which a netbook PC controls the autosampler and cytometers, respectively. (**b**) Close-up of the four sampling probes during processing of a 1,536-well plate. (**c**) Parallel sampling pattern from left to right and top to bottom of the four 384-well segments of a 1,536-well plate, each segment analyzed by the indicated cytometer. (**d**) Histogram of the red fluorescence distribution of five color-coded sets of microspheres representing pooled data from all wells and cytometers collected from a 1,536-well plate. (**e**) Time-resolved display of five-plex microsphere data from 1,536-well plate analysis in which data from each cytometer as indicated are linked together for display in a single plot (bottom). Although collected in parallel, data from each cytometer are displayed side-by-side on a common Microplate Wells axis for better visual comparison. Zoomed-in 50-s plot sections (top, ~ 30 wells each) illustrate the uniformity of resolution by each cytometer of bead sets (red fluorescence intensity axis) and well content (gap-separated clusters on the Microplate Wells axis) across the plate. Additional gating information is shown in Supporting Information Figure 2. [Color figure can be viewed in the online issue which is available at wileyonlinelibrary.com]

decreases. Positive control wells represented the maximum expected MFI in the former case, the minimum in the latter, and vice-versa for negative control wells. For the purposes of calculating Z', the important consideration was only that control wells with minimum and maximum MFI be distinguished as follows:

$$Z' = 1 - \{([3\times SD_{MAX}] + [3\times SD_{MIN}]/(Mean_{MAX} - Mean_{MIN})\}$$

where $Mean_{MAX}$ and SD_{MAX} represent the mean and SD of MFI values from control wells with maximum MFI, and $Mean_{MIN}$ and SD_{MIN} are the same for control wells with minimum MFI. Possible values of Z' range from negative infinity to 1.0. An assay is deemed excellent for screening purposes if Z' is in the range between 0.5 and 1.0. A Z' value of 0 is indicative of a screening assay capable of providing only a "yes/no" type of output.

An alternative statistic is the *Z*-factor, which is calculated in a similar fashion as Z' except that (1) the terms in the equation pertaining to the negative control wells are substituted with mean and SD MFI values for all wells in the plate excluding the positive control wells and (2) the absolute value of the difference term in the denominator is used. The *Z*-factor is subject to influence from a variety of additional factors that do not affect Z' such as compound concentration and number of active compounds on the plate. As the value of Z' is subject to fewer nuances of interpretation than the *Z*-factor, we exclusively used Z' for the purposes of evaluating instrument performance in the present studies.

Flow Cytometry

All analyses were performed with Accuri C6 flow cytometers (see above). Singlet populations of cells and microspheres were selectively gated for the analysis on the basis of forward light scatter (linear scale) and side light scatter (log scale) from a 488-nm laser. Green fluorescence emission detected at 533/30 nm was excited by a 488-nm laser, recorded in the FL1-H channel, and displayed in log scale. Red fluorescence emission detected at 675/25 was excited by a 640-nm laser, recorded in the FL4-H channel, and displayed in log scale. Representative list mode and GatingML files for any of the figures are available upon request from the corresponding author.

Results

Cluster Cytometry

The platform consisted of a high-precision positioning autosampler, a cluster of four small-footprint, moderate-cost Accuri C6 flow cytometers, and a four-channel peristaltic pump that delivered samples from four sample uptake probes to each of the flow cytometers (Fig. 1a and Supporting Information Fig. 2). The cytometers were remotely controlled over an Ethernet network by a netbook computer that coordinated

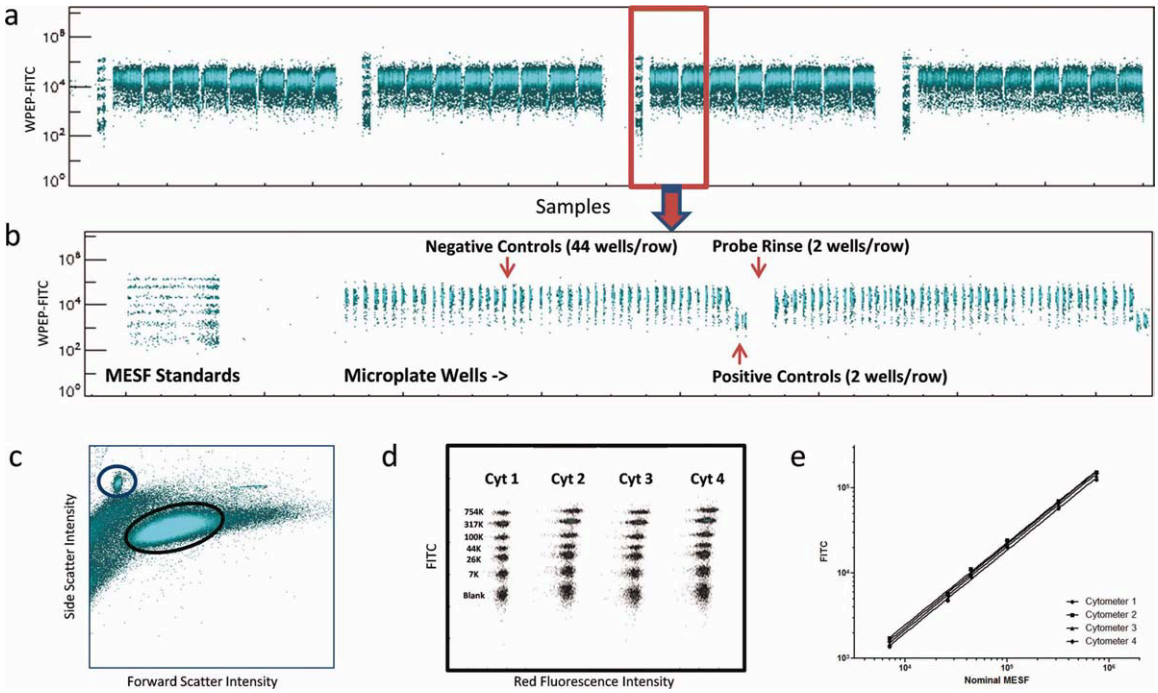

Figure 2. FPR ligand-binding assay analysis. U937 cells expressing FPR were incubated with green fluorescent FPR ligand (WPEP—FITC) in the presence (positive control wells) or absence (negative control wells) of a nonfluorescent FPR ligand (fMLFF). (**a**) Plot of linked samples data from all cytometers. (**b**) Zoomed-in region illustrating the initial 10-s sampling of calibration standard microspheres (MESF standards) followed by sampling of microplate wells. Indicated are gap-separated samples from the first 48-well row in which the first 44 are negative control wells, the next two are positive control wells, and the last two are rinse wells (no cells). (**c**) Scatter plot (forward and side scatter from the 488-nm laser) of data pooled from all wells and cytometers illustrating electronic gates used to distinguish U937 cells (ellipse in center) and calibration standards microspheres (top left circle). (**d**) Green fluorescence distribution of the calibration standards microspheres from the four cytometers. Labels at top indicate the cytometer and at left the MESF corresponding to microsphere clusters resolved on the FITC axis. A two-parameter dot-plot display was used to illustrate homogeneity of the microsphere populations. Red fluorescence intensity was used as the *x*-axis parameter to demonstrate that there was little or no FITC fluorescence spillover into the red fluorescence channel used to distinguish red fluorescent microsphere sets in Figures 1 and 3. (**e**) Log—Log plots of MESF vs. FITC green fluorescence intensity of calibration standards microspheres recorded by each cytometer. Lines fitted by linear regression were used to transform cell WPEP—FITC data from each well to calibrated MESF for the analysis reported in Table 1 and Supporting Information Figure 5. Detailed gating information and a schematic illustrating the assay principles are shown in Supporting Information Figure 3. [Color figure can be viewed in the online issue which is available at wileyonlinelibrary.com]

autosampler and cytometer operation, file naming via barcode reader, and data streaming to a centralized storage location where data from the four cytometers were linked and analyzed (Fig. 1a). To enable high-throughput analysis of samples displayed in 1,536-well plate format, the four sample uptake probes were positioned at eight-well intervals across the 32-row dimension of the plate (Fig. 1b). The autosampler moved the 4-probe head across the 48-column plate dimension row-by-row so that each probe sampled a 384-well segment of the plate (Fig. 1c). In initial pilot tests, a multiplexed preparation of microspheres consisting of five sets with distinctive red fluorescence intensity profiles (Fig. 1d) was dispensed into a 1,536-well plate so that each well contained 2,000 microspheres from each set in a 10-μL volume. Approximately, 2 μL was aspirated per well from each plate segment in parallel at a rate that allowed the entire plate to be processed in $<$11 min. In a representative experiment, each cytometer consistently resolved the samples from individual wells as well as the five discrete fluorescence profiles of microspheres in each sample (Fig. 1e). The number of microspheres detected from each of the five fluorescence intensity sets averaged from 299 $\pm$ 34 to 328 $\pm$ 31 per well over the entire plate and ranged from a minimum of 108 to a maximum of 429 from each set per well.

Cluster Cytometer Performance

Performance of the HyperCyt platform has been extensively validated for both cell and microsphere based HTS assays in 96- and 384-well format. However, the move to 1,536-well plates and use of multiple flow cytometers in parallel accentuated several new technical issues: the need to restrict assay volumes to 10 μL or less to accommodate smaller wells, limited options for ensuring adequate mixing of reagents and suspension of cells and particles in such small wells, the potential need to detect and correct for differences in the performance of individual flow cytometers, and the ability to reanalyze a plate in the event of problems encountered with one or more of the cytometers (e.g., clogging) during the primary analysis. To address these issues, we used cell- and microsphere-based HTS assays that had been well characterized in the previous studies.

Table 1. Evaluation of the FPR fluorescent ligand-binding assay in 1536-well format

		WPEP–FITC (MFI)				CALIBRATED MESF			
CYTOMETER	CONTROL[A]	MEAN	SD	CV	Z'	MEAN	SD	CV	Z'
1	Pos	2,080	96	4.6	0.579	10,390	492	4.7	0.572
	Neg	22,378	2,750	12.3		120,176	15,183	12.6	
2	Pos	2,140	64	3.0	0.819	8,544	265	3.1	0.815
	Neg	23,067	1,199	5.2		100,825	5,428	5.4	
3	Pos	2,032	44	2.2	0.819	9,350	207	2.2	0.816
	Neg	23,522	1,254	5.3		114,534	6,240	5.4	
4	Pos	1,895	100	5.3	0.704	8,108	437	5.4	0.699
	Neg	23,130	1,998	8.6		105,542	9,324	8.8	
All	Pos	2,036	119	5.9	0.704	9,098	947	10.4	0.605
	Neg	23,024	1,950	8.5		110,293	12,389	11.2	

[a] Plate segments analyzed by each cytometer contained 352 negative control wells and 16 positive control wells.

Cell Suspension, Mixing, and Cross-cytometer Fluorescence Response Calibration

The FPR ligand-binding inhibition assay, successfully used to identify high-affinity, small-molecule FPR antagonists (24,28), tests the ability of compounds to displace a fluorescent peptide ligand, WPEP–FITC, from FPRs expressed in membranes of intact cells (23,29) (Supporting Information Fig. 3d). The original assay volume of 15 μL was reduced to 10 μL by increasing cell and reagent concentrations. Three sequential rounds of droplet deposition with a microdispenser were used to fill wells first with control solutions with or without receptor blocking peptide ligand (4 μL), then cells (3 μL) and finally, WPEP–FITC fluorescent ligand. All mixing in wells was exclusively accomplished by rotating the plates end-over-end from inverted to upright position at ~4 rpm during each incubation step as described previously (30). Plates were set up with 44 wells of each row as negative controls (cells plus WPEP–FITC to produce brightly fluorescent cells) and 2 as positive controls (cells and WPEP–FITC plus excess nonfluorescent, blocking peptide ligand to produce dimly fluorescent cells). The four sampling probes were programmed to aspirate a suspension of fluorescein calibration standard microspheres for 10 s prior to sampling of the 1,536-well plate. Thus, the analysis results for each cytometer/plate segment had a calibration standards fluorescence profile as an internal control of cytometer fluorescence response performance (Figs. 2a and b). The calibration standard microspheres had a distinctive light-scattering profile (Fig. 2c) by which they could be distinguished from the cells and gated for separate analysis (Supporting Information Figs. 3a–c). Comparison of the resulting fluorescence calibration curve profiles for the four flow cytometers indicated a high degree of similarity (Figs. 2d and e).

In a representative plate, a greater than tenfold response difference between positive and negative controls was observed for each of the four cytometer/plate segments (Table 1). Z' scores (27) calculated separately for each cytometer/plate segment on the basis of WPEP–FITC green fluorescence intensity ranged from 0.579 to 0.819. When data from the four segments were pooled, as if the entire plate had been analyzed by a single flow cytometer, the Z' score was 0.704. Transformation to a calibrated scale such as MESF is an accepted means of normalizing data to compensate for differences between relative fluorescence response values produced by different flow cytometers. Using regression coefficients from line fits shown in Fig. 2d, calibrated MESF values were calculated for control well data. Unexpectedly, such a transformation resulted in a slightly lower Z' score for pooled data (0.605) in association with increased coefficients of variation (CVs) for positive and negative controls (Table 1).

To further address this issue, we plotted calibrated MESF values for both calibration microspheres and cells as a function of nominal MESF for the four cytometers (Supporting Information Fig. 5a). Calibrated MESF profiles and fitted regression lines for the calibration microspheres were virtually identical for all cytometers, an indication that the linear fit model brought all cytometers into good quantitative agreement. By contrast, the calibrated MESF values for cells from control wells were less tightly grouped about the overlapping best fit lines and showed relatively small but statistically significant intercytometer differences within each control group. These measurements were made on the basis of the height of the fluorescence pulse produced by cell or microsphere passage through the laser beam (FL1-H). Such measurements can be sensitive to differences in laser beam configuration between cytometers (e.g., laser beam diameter), particularly when making quantitative comparisons between particles of different diameters as was the case for the microspheres and cells (~ 5 vs. ~ 9 μm, respectively). Therefore, we also investigated the use of fluorescence pulse area measurements (FL1-A) that are considered less sensitive to this potential source on intercytometer variation (Supporting Information Fig. 5b). Although negative control values appeared to group more tightly in FL1-A plots as compared to FL1-H plots, positive control values did not exhibit a similar trend (Supporting Information Fig. 5b). It seems likely that plate position effects may have accounted for some of the observed variations, perhaps reflecting assay artifacts owing to edge effects or reagent dispensing variation across the four quadrants of the 1536-well plate.

Taken together, these results suggested that the innate variation between the four flow cytometers was relatively small

and subject to the sources of variation that could not be improved by MESF transformation of fluorescence data. Clearly documented was the importance of including assay control wells in all plate quadrants and using fluorescence data from them as the primary means for normalizing results individually for each cytometer. The relative uniformity and signal range of assay response values over the entire plate indicated that adequate mixing had been accomplished without a need for physical interventions such as pipetting or vortexing of assay suspensions. This was confirmed by Z' scores of 0.780, 0.781, and 0.830 that were obtained when three additional plates were analyzed separately in a similar fashion (pooled WPEP–FITC control well MFI data from the four segments of each plate, data not shown).

Analysis Repeatability

We have previously described microsphere-based HTS assays to detect the inhibitors of proteases, anthrax LF, and Botulinum neurotoxin A light chain (BoNT/ALC) (14,25,26). The assays employ recombinant fusion proteins consisting of a protease substrate sequence (peptide with cleavage site) fused at one end with a biotinylated attachment sequence and at the other with GFP. The substrate fusion proteins are attached to color-coded streptavidin microspheres via the biotin moiety and protease activity is detected as a loss of microsphere GFP fluorescence intensity, resulting from cleavage of bound substrate (Supporting Information Fig. 4a). To adapt the protease assay to 1,536-well plates, we reduced assay volumes from the original 20–25 to 10 μl by concentrating assay components as above. To two plates, we separately dispensed the mixtures of proteases (LF and BoNT/ALC) and color-coded microspheres bearing GFP fusion proteins (LF substrate, BoNT/ALC substrate and a protein resistant to both proteases). We used a 1,536 pintool set to add 1,993 test compounds from the Molecular Libraries Small Molecule Repository (MLSMR) Validation Set (100 nL/well). The plates were incubated overnight on the plate rotator to allow protease reactions to go to completion and processed the following day. Detailed results of the compound screen, which also evaluated an additional protease and microsphere-bound substrate in each well, will be reported separately (PubChem Summary AIDs 566467, 566469, and 566470, updated at the completion of each screening stage); however, we took the opportunity to assess the repeatability of results by processing each plate three times in succession.

From 1,492 wells on each plate, the mean, SD, and corresponding CV were determined for the three sequential measurements of median green fluorescence intensity of each microsphere set in the well. In histograms plotting the distribution of CVs for each set, the 95th percentiles ranged from 4.6% for LF substrate to 5.4% for BoNT/ALC substrate (Fig. 3). Thus, 95% or more of the replicate measurements for each bead set had CVs of $<6\%$. For substrates susceptible to protease cleavage, Z' scores derived from positive and negative control wells (eight of each per plate segment) averaged 0.73 (LF) and 0.86 (BoNT/ALC) over the 24 separate plate segment determinations (Figs. 3b and c, eight segments of two plates evaluated three times each). These results indicated that the same plate can be analyzed up to three times with the expectation of consistently good data quality and reproducibility.

Validation Against 384-Well Plate Data

Under the auspices of the NIH-sponsored Molecular Libraries Screening Centers Network and Probe Production Centers Network (MLSCN and MLPCN, respectively), the single-cytometer HyperCyt system has been applied to the screening of small molecules from the MLSMR in more than 18 campaigns (>40 separate biological targets) involving a diversity of cell- and microsphere-based assays. To date, our flow cytometry screening has been exclusively performed in 384-well format. To validate the performance of the Cluster Cytometer platform, we selected a microsphere-based assay that had recently been screened in 384-well format. The assay was designed to detect the inhibitors selectively targeting GRK2, an enzyme implicated in cardiac failure (31). In the HTS assay, a green fluorescent RNA aptamer is used in a displacement assay to identify small molecules that bind to the regions of the GRK2 kinase domain critical for activity (Fig. 4a). Biotin-GRK2 is bound to streptavidin microspheres so that the microspheres become brightly fluorescent in the presence of the aptamer. Hit detection is based on a decrease in microsphere fluorescence intensity that results when a test compound disrupts aptamer binding to GRK2 (Fig. 4b and http://pubchem.ncbi.nlm.nih.gov/assay/assay.cgi?aid=488855).

When Cluster Cytometer HTS was performed in 1,536-well format using the MLSMR Validation Set, 14 compounds inhibited aptamer binding to GRK2 by 25% or more (Fig. 4b and Table 2). Of these, seven inhibited similarly in two separate HTS campaigns performed in the low-density, 384-well plate format (Table 2, confirmed), first in a screen of the Validation Set (PubChem AID 488806) and subsequently in a screen of the full MLSMR library in which most of the Validation Set compounds are represented (327,943 compounds, PubChem AID 488847). There was one compound that had activity in the two single-cytometer screens but not in the Cluster Cytometer screen; however, it failed to inhibit in a follow-up confirmation screen (PubChem AID 504451) and was considered a false positive (Table 2, compound ID 448222). There were four compounds that were apparent hits in the Cluster Cytometer screen but not in the single-cytometer screen. We interpreted these hits as likely false positives as the compounds were consistently inactive in the single-cytometer screens. We have not analyzed these compounds further. Thus, HTS in high-density plate format with the Cluster Cytometer HyperCyt platform detected all compounds in the Validation Set for which activity had been previously confirmed using our conventional single-cytometer HTS platform.

Discussion

The concept of using multiple flow cytometers in parallel has some precedence in the recent past, applied primarily as an approach to boost throughput of cell isolation and purifi-

Table 2. Validation of hit detection in HTS

		INHIBITION OF APTAMER-3′-FAM BINDING (%)			
RESULTS IN 384-WELL HTS	COMPOUND ID	AID[A] 488806	AID 488847	AID 504451	1,536-WELL HTS
Confirmed (All >25%)	16195270	92	88		94
	6763	67	28		88
	1780	62	50		55
	460749	45	34		66
	5702697	39	89		66
	646406	34	47		29
	6420073	92	ND[b]		99
False positive (One <25%)	2957802	86	11		75
	906542	61	0		82
	2827740	33	0		38
	448222	66	30	1	0
Negative (All <25%)	2936792	2	4		98
	1522903	0	0		97
	104871	5	2		57
	12035	5	2		52

[a] PubChem assay ID for 384-well plate HTS results.
[b] ND, Not done.

cation operations by fluorescence-based cell sorting. An example is the commercial use of banks of high-speed cell sorters running continuously in parallel to separate *X*- and *Y*-chromosomes bearing sperm for use by breeders of domestic animals (e.g., www.sexingtechnologies.com/). Cell-sorting flow cytometers are now commercially available in which up to four sorting modules can be packed into the footprint of one traditional instrument and operated in parallel over remote network connections to speed up the purification of rare cell subpopulations (www.i-cyt.com). Our integrated, multiple flow cytometer screening platform now extends the parallel flow cytometry concept to speed up performance and analysis of large numbers of discrete biological experiments involving cell and particle suspensions.

We have found cluster cytometry to offer a number of benefits as compared to the alternate approach of operating four separate flow cytometry screening platforms in parallel. (1) Screening lab space requirement is significantly reduced. (2) The close proximity of cytometers and sample delivery systems makes it more practical for the screening process to be effectively implemented and monitored by a single operator. (3) Synchronization of sample processing by the four cytometers facilitates automated "just-in-time" analysis of screening assay data. In practice, we routinely produce a complete analysis of the screening data for each plate (Z', hit frequency, number of cells/well, etc.) within the 10–12 min time required to process the next plate. This allows rapid detection of problems that might not be obvious by visual inspection so that they can be quickly fixed. Affected plates are then placed back on the rotating suspension system for later reanalysis. (4) There is a single point of plate introduction rather than four separate locations, more efficient for interfacing with an automated plate transport system. (5) There is flexibility of operating modes. The platform can be easily switched to run 1, 2, 3, or 4 flow cytometers at a time and can accommodate microplates of various well configurations (e.g., 96, 384, 12, 24, etc.).

A potential disadvantage of the cluster cytometer approach would be the consequences of a malfunctioning flow cytometer or autosampler. One possible solution for accommodating cytometer failure would be to switch to two-cytometer operating mode and process the two halves of a 1,536-well plate in parallel. However, the modularity and moderate cost of the Accuri C6 flow cytometer lends feasibility to an alternate solution: having a backup unit available that can be quickly swapped for a malfunctioning unit in the event of an instrument problem that resists quick diagnosis and repair. We have shown this to work in practice when the red laser on one of the cytometers failed in the middle of a major screening operation. It took only $\sim$ 15 min to swap in a backup unit to allow successful completion of the screen. We also have a backup autosampler (considerably less expensive than a flow cytometer) that can be swapped for the original in $\sim$ 15 min in the event, rare in our experience, and that the robotic sample handling component might fail. Thus, with appropriate backup infrastructure recovery from failure has similar time requirements whether operating in cluster or single-cytometer mode.

An important issue for the cluster cytometer approach was the need to evaluate equivalency of fluorescence responses between flow cytometers and to have methods to correct for potential interunit variability. In this study, we used calibration standard microspheres to evaluate FITC fluorescence response equivalency of the cytometers. All showed linear fluorescence response profiles with parallel but offset regression lines, an indication that there were differences in fluorescence response sensitivity reflecting the ability to resolve dim fluorescence in the FITC channel (Fig. 2e). It was expected that

transformation of all fluorescence response data to the MESF scale would suffice to ensure equivalency. This was indeed the case for microsphere FITC fluorescence results (Supporting Information Fig. 5). However, extended analysis of cell fluorescence data from control wells in the FPR ligand-binding assay clearly showed that there were other sources of variability such as putative plate position effects that may not have been attributable to instrument performance differences. These contributed to apparent disparities between cytometers that could not be entirely resolved by MESF transformation (Supporting Information Fig. 5). We conclude that a more robust method for achieving quantitatively comparable results is to include control wells in common for each cytometer that define assay response limits (e.g., maximum and minimum response), graded response output levels (e.g. different concentrations of a response modulating chemical) or other response level benchmarks. Fluorescence data from these wells can then serve as a basis for normalizing results individually for each cytometer to a common scale suitable for crosscomparison such as % inhibition, % response relative to a control source of cells, % response relative to a curve produced by a control chemical, and so on. The same considerations apply for any fluorescence channel in which the making of quantitative fluorescence response comparisons is of interest. If compensation is required to correct for fluorescence spillover between channels, common compensation controls are used to set up the cytometers to produce similar results prior to sample processing. Common assay control wells are then used to normalize results postanalysis. In the cluster cytometry approach, as in any studies involving a collection of flow cytometers running a common assay (e.g., multi-institutional collaborations), the low end of fluorescence intensity amenable to analysis will be governed by the least sensitive instrument. An advantage of the cluster approach is that all flow cytometers are evaluated in parallel under the same experimental conditions so that limiting conditions can be rapidly and unambiguously identified.

The present results demonstrate that bioassays involving both cell and microsphere suspensions can be successfully performed and analyzed in high-density, 1,536-well format with robustness in quality and repeatability critical for the HTS environment. Since the completion of these pilot studies, the Cluster Cytometer HyperCyt platform has been successfully

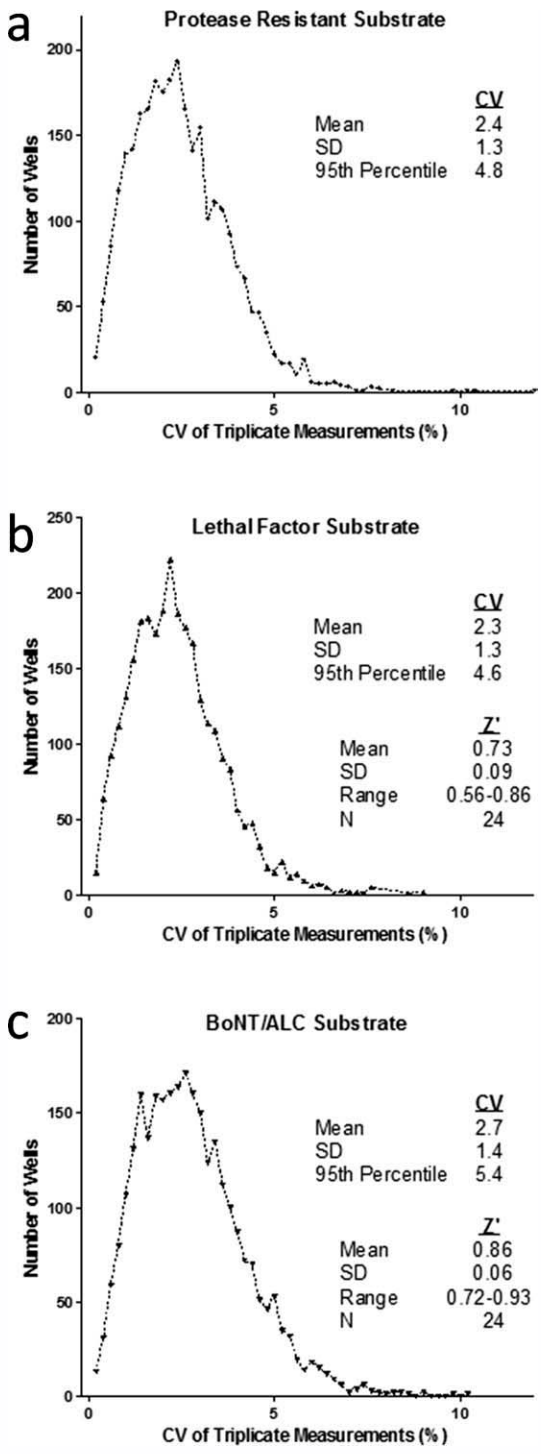

Figure 3.

Figure 3. Data acquisition and analysis repeatability. A protease inhibition assay screen was performed in which two 1,536-well plates were sequentially processed three times each to determine repeatability of fluorescence measurements. Wells contained three color-coded bead sets to which were attached a protease resistant substrate or substrates selectively cleaved by *B. anthracis* LF or *C. botulinum* neurotoxin A light chain (BoNT/ALC). All wells except negative control wells contained a mixture of LF and BoNT/ALC proteases in the presence or absence of small-molecule test compounds. Substrates were labeled with GFP so that cleavage by protease resulted in a decrease of microsphere green MFI. Illustrated are the distributions of CV of the replicate MFI determinations from 1,492 wells for (**a**) protease resistant, (**b**) LF sensitive, and (**c**) BoNT/ALC-sensitive substrates. CV = 100 × MFI SD/MFI mean. Indicated in each panel are the mean, SD, and 95th percentile of the CV distribution. For protease sensitive substrates (b and c), *Z'* scores were calculated from MFI determinations in the presence and absence of protease (control wells to which compounds were not added). Indicated are the mean, SD, and range of the 24 *Z'* scores (four-plate segments from two plates measured three times each). Details of flow cytometry gating strategy and an assay schematic are shown in Supporting Information Figure 4.

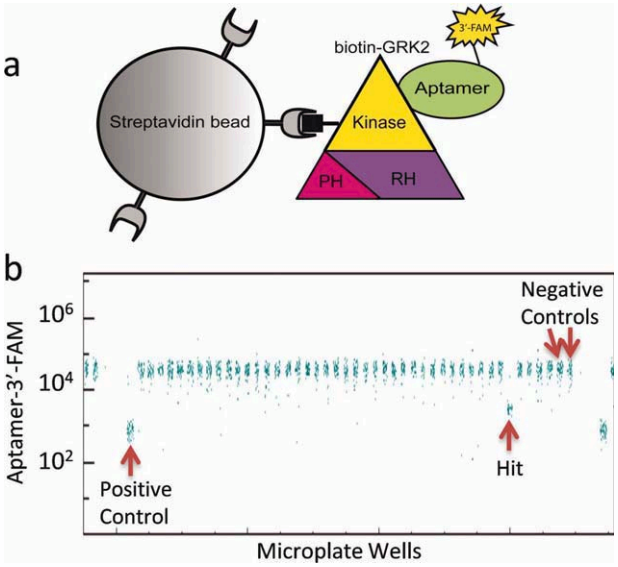

Figure 4. GRK2 assay. (**a**) Biotin-GRK2 is bound to streptavidin microspheres and incubated with a green fluorescent RNA aptamer, aptamer-3′-FAM, in the presence of test compounds. The HTS assay detects small molecules that bind to the GRK2 kinase domain and displaces aptamer-3′-FAM. RH, regulator of G-protein signaling homology domain. PH, pleckstrin homology domain. (**b**) A zoomed-in region of data from the HTS assay illustrating the decrease in microsphere aptamer-3′-FAM fluorescence observed in positive control wells containing excess nonfluorescent aptamer as compared to negative control wells containing buffer alone. Also illustrated is a well that contained a compound that significantly inhibited aptamer-3′-FAM binding (Hit). [Color figure can be viewed in the online issue which is available at wileyonlinelibrary.com]

used for HTS of a multiplexed assay to detect the inhibitors of three proteases (referenced above) against the full MLSMR library of more than 350,000 small molecules (PubChem Summary AIDs 566467, 566469, and 566470). After a preliminary series of smaller shakedown runs, we routinely screened more than 51,000 compounds (60,000 wells when including controls and rinse wells) per day.

This technology complements the capabilities of imaging-based platforms that have been successfully used for high content, high-throughput analyses of surface-attached cells. Moreover, it is uniquely positioned to augment rapidly expanding suspension array and fluorescent cell barcoding technologies in which as many as 100 bioassays are performed in a single well (32,33). We have successfully implemented a number of such multiplexed assays for HTS campaigns in single flow cytometer, 384-well plate format. Recently documented examples include a fluorescently "barcoded" five-plex of cell strains from the Yeast-GFP collection to probe Target-of-Rapamycin signaling pathways (34) (PubChem AID 1867) and a six-plex of color-coded microspheres to probe BCL-2 family protein binding interactions (35,36) (PubChem AID 1908). A relatively modest 10-plex bioassay performed in high-density format can be expected to produce over 15,000 distinct and quantitative experimental measurements in <11 min from a single 1,536-well plate. It seems likely that large-scale bioassay multiplexing capabilities will prove a useful tool for probing complex systems of biomedical importance such as signaling networks, drug selectivity, crossreactivity, and so on. Of additional importance is our demonstration that such versatility can be achieved with relatively low cost but powerful, small-footprint flow cytometers that have only recently become commercially available. The advent of the low-cost personal computer enabled the implementation of parallel computing systems as an affordable approach for resolving large-scale computational problems. We anticipate that a similar trend will lead to cluster cytometry as a practical approach, affordable to a broader segment of the worldwide research community, for addressing large-scale studies of biological complexity. Parallel-channel, chip-based microfluidic sorting systems are currently in development that promise to further extend the throughput capabilities of parallel flow cytometry (e.g., www.cytonome.com), and it will be of great interest to see how performance, versatility, failure-mode recovery options, and costs of such systems will compare with modular systems such as reported here.

Acknowledgments

The authors gratefully acknowledge Matthew Hess and Aaron Kennington of IntelliCyt Corp. for helpful discussions about software for implementing Ethernet network communications protocols.

Literature Cited

1. Giuliano KA, DeBiasio RL, Dunlay RT, Gough A, Volosky JM, Zock J, Pavlakis G, Taylor DL. High-content screening: A new approach to easing key bottlenecks in the drug discovery process. J Biomol Screen 1997;2:249–259.
2. Haney SA, LaPan P, Pan J, Zhang J. High-content screening moves to the front of the line. Drug Discov Today 2006;11:889–894.
3. Kuckuck FW, Edwards BS, Sklar LA. High throughput flow cytometry. Cytometry 2001;44:83–90.
4. Arterburn JB, Oprea TI, Prossnitz ER, Edwards BS, Sklar LA. Discovery of selective probes and antagonists for G-protein-coupled receptors FPR/FPRL1 and GPR30. Curr Top Med Chem 2009;9:1227–1236.
5. Sklar LA, Edwards BS. HTS flow cytometry, small molecule discovery, and the NIH Molecular Libraries Initative. In: Litvin V, Marder P, editors. Flow Cytometry in Drug Discovery and Development, Hoboken, NJ: John Wiley & Sons; 2010. pp71–98.
6. Jackson WC, Bennett TA, Edwards BS, Prossnitz E, Lopez GP, Sklar LA. Performance of in-line microfluidic mixers in laminar flow for high-throughput flow cytometry. Biotechniques 2002;33:220–226.
7. Jackson WC, Kuckuck F, Edwards BS, Mammoli A, Gallegos CM, Lopez GP, Buranda T, Sklar LA. Mixing small volumes for continuous high-throughput flow cytometry: Performance of a mixing Y and peristaltic sample delivery. Cytometry 2002;47:183–191.
8. Bologa CG, Revankar CM, Young SM, Edwards BS, Arterburn, JB, Kiselyov AS, Parker, MA, Tkachenko SE, Savchuck NP, Sklar LA, Oprea TI, and Prossnitz ER. Virtual and biomolecular screening converge on a selective agonist for GPR30. Nat Chem Biol 2006;2:207–212.
9. Bartsch JW, Tran HD, Waller A, Mammoli AA, Buranda T, Sklar LA, Edwards BS. An investigation of liquid carryover and sample residual for a high-throughput flow cytometer sample delivery system. Anal Chem 2004;76:3810–3817.
10. Young SM, Curry MS, Ransom JT, Ballesteros JA, Prossnitz ER, Sklar LA, Edwards BS. High-throughput microfluidic mixing and multiparametric cell sorting for bioactive compound screening. J Biomol Screen 2004;9:103–111.
11. Haynes MK, Strouse JJ, Waller A, Leitao A, Curpan RF, Bologa C, Oprea TI, Prossnitz ER, Edwards BS, Sklar LA, Thompson TA. Detection of intracellular granularity induction in prostate cancer cell lines by small molecules using the HyperCyt high throughput flow cytometry system. J Biomol Screen 2009;14:596–609.
12. Young SM, Bologa C, Prossnitz ER, Oprea TI, Sklar LA, Edwards BS. High-throughput screening with HyperCyt flow cytometry to detect small molecule formylpeptide receptor ligands. J Biomol Screen 2005;10:374–382.
13. Edwards BS, Young SM, Oprea TI, Bologa CG, Prossnitz ER, Sklar LA. Biomolecular screening of formylpeptide receptor ligands with a sensitive, quantitative, high-throughput flow cytometry platform. Nat Protoc 2006;1:59–66.
14. Saunders MJ, Kim H, Woods TA, Nolan JP, Sklar LA, Edwards BS, Graves SW. Microsphere-based protease assays and screening application for lethal factor and factor Xa. Cytometry Part A 2006;69A:342–352.

15. Edwards BS, Ivnitski-Steele I, Young SM, Salas VM, Sklar LA. High-throughput cytotoxicity screening by propidium iodide staining. Curr Protoc Cytom 2007; Chapter 9:Unit 9.24.
16. Simons PC, Young SM, Gibaja V, Lee WC, Josiah S, Edwards BS, Sklar LA. Duplexed, bead-based competitive assay for inhibitors of protein kinases. Cytometry Part A 2007;71A:451–459.
17. Dennis MK, Bowles HJ, MacKenzie DA, Burchiel SW, Edwards BS, Sklar LA, Prossnitz ER, Thompson TA. A multifunctional androgen receptor screening assay using the high-throughput Hypercyt flow cytometry system. Cytometry Part A 2008;73A:390–399.
18. Ivnitski-Steele I, Larson RS, Lovato DM, Khawaja HM, Winter SS, Oprea TI, Sklar LA, Edwards BS. High-throughput flow cytometry to detect selective inhibitors of ABCB1, ABCC1, and ABCG2 transporters. Assay Drug Dev Technol 2008;6:263–276.
19. Winter SS, Lovato DM, Khawaja HM, Edwards BS, Steele ID, Young SM, Oprea TI, Sklar LA, Larson RS. High-throughput screening for daunorubicin-mediated drug resistance identifies mometasone furoate as a novel ABCB1-reversal agent. J Biomol Screen 2008;13:185–193.
20. Surviladze Z, Waller A, Wu Y, Romero E, Edwards BS, Wandinger-Ness A, Sklar LA. Identification of a small GTPase inhibitor using a high-throughput flow cytometry bead-based multiplex assay. J Biomol Screen 2010;15:10–20.
21. Prossnitz ER. Desensitization of N-formylpeptide receptor-mediated activation is dependent upon receptor phosphorylation. J Biol Chem 1997;272:15213–15219.
22. Strouse JJ, Young SM, Mitchell HD, Ye RD, Prossnitz ER, Sklar LA, Edwards BS. A novel fluorescent cross-reactive formylpeptide receptor/formylpeptide receptor-like 1 hexapeptide ligand. Cytometry Part A 2009;75A:264–270.
23. Edwards BS, Young SM, Oprea TI, Bologa C, Prossnitz E, Sklar LA. Biomolecular screening of formylpeptide receptor ligands with a sensitive, quantitative, high-throughput flow cytometry platform. Nat Protoc 2006;1:59–66.
24. Young SM, Bologa CM, Fara D, Bryant BK, Strouse JJ, Arterburn JB, Ye RD, Oprea TI, Prossnitz ER, Sklar LA, et al. Duplex high-throughput flow cytometry screen identifies two novel formylpeptide receptor family probes. Cytometry Part A 2009;75A:253–263.
25. Saunders MJ, Edwards BS, Zhu J, Sklar LA, Graves SW. Microsphere-based flow cytometry protease assays for use in protease activity detection and high-throughput screening. Curr Protoc Cytometry 2010; Chapter 13:Unit 13.12.1–13.12.17.
26. Saunders MJ, Graves SW, Sklar LA, Oprea TI, Edwards BS. High-throughput multiplex flow cytometry screening for botulinum neurotoxin type a light chain protease inhibitors. Assay Drug Dev Technol 2010;8:37–46.
27. Zhang JH, Chung TD, Oldenburg KR. A simple statistical parameter for use in evaluation and validation of high throughput screening assays. J Biomol Screen 1999;4:67–73.
28. Edwards BS, Bologa C, Young SM, Balakin KV, Prossnitz E, Savchuck NP, Sklar LA, Oprea TI. Integration of virtual screening with high throughput flow cytometry to identify novel small molecule formylpeptide receptor antagonists. Mol Pharmacol 2005;68:1301–1310.
29. Edwards BS, Young SM, Ivnitsky-Steele I, Ye RD, Prossnitz ER, Sklar LA. High-content screening: Flow cytometry analysis. Methods Mol Biol 2009;486:151–165.
30. Ramirez S, Aiken CT, Andrzejewski B, Sklar LA, Edwards BS. High-throughput flow cytometry: Validation in microvolume bioassays. Cytometry A 2003;53A:55–65.
31. Rockman HA, Chien KR, Choi DJ, Iaccarino G, Hunter JJ, Ross J, Jr., Lefkowitz RJ, Koch WJ. Expression of a beta-adrenergic receptor kinase 1 inhibitor prevents the development of myocardial failure in gene-targeted mice. Proc Natl Acad Sci USA 1998;95:7000–7005.
32. Nolan JP, Sklar LA. Suspension array technology: Evolution of the flat-array paradigm. Trends Biotechnol 2002;20:9–12.
33. Krutzik PO, Nolan GP. Fluorescent cell barcoding in flow cytometry allows high-throughput drug screening and signaling profiling. Nat Methods 2006;3:361–368.
34. Chen J, Young SM, Allen CP, Seeber A, Péli-Gulli M-P, Panchaud N, Waller A, Ursu O, Yao T, Golden JE, et al. Identification of a small molecular inhibitor of yeast TORC1 using a flow cytometry based multiplex screen. ACS Chem Biol 2012; Feb 1 [Epub ahead of print].
35. Curpan RF, Simons PC, Zhai D, Young SM, Carter MB, Bologa CG, Oprea TI, Satterthwait AC, Reed JC, Edwards BS, et al. High-throughput screen for the chemical inhibitors of antiapoptotic Bcl-2 family proteins by multiplex flow cytometry. Assay Drug Dev Technol 2011;9:465–474.
36. Simons PC, Young SM, Carter MB, Waller A, Zhai D, Reed JC, Edwards BS, Sklar LA. Simultaneous in vitro molecular screening of protein-peptide interactions by flow cytometry, using six Bcl-2 family proteins as examples. Nat Protoc 2011;6:943–952.